Journal of Experimental Pharmacology

Dovepress
Taylor & Francis Group

Open Access Full Text Article

ORIGINAL RESEARCH

In vivo Therapeutic Inhibition of the Tp53-Induced Glycolysis and Apoptosis Regulator (TIGAR) by Intravenous Administration of an Anti-Oncological siRNA-Biopolymer, TI6752 (Tituxistatin), in a Preclinical Xenograft Model of Colorectal Cancer

Carolyn K Harrod[1], Brenda Y Hernandez[2], Courtney Yates[3], Robert Harrod[1]

[1]Department of Biological Sciences and The Dedman College Center for Drug Discovery, Design & Delivery, Southern Methodist University, Dallas, TX, USA; [2]Hawaii Tumor Registry, University of Hawaii Cancer Center, Honolulu, HI, USA; [3]Laboratory Animal Resource Center, Southern Methodist University, Dallas, TX, USA

Correspondence: Robert Harrod, Department of Biological Sciences and The Dedman College Center for Drug Discovery, Design & Delivery, Southern Methodist University, 6501 Airline Drive, 334-DLS, Dallas, TX, 75275-0376, USA, Tel +1 214 768 3864, Fax +1 214 768 3955, Email rharrod@smu.edu

Introduction: The TP53-induced glycolysis and apoptosis regulator (TIGAR) is upregulated in many cancers and often correlates with poor clinical prognoses and serves as a key determinant of therapy-responsiveness. The TIGAR protein is structurally nearly identical to the phosphatase subunit of the bifunctional, fructose-6-phosphokinase/fructose-2,6-bisphosphatase, which has likely hindered efforts to date to develop small-molecule pharmacological inhibitors of TIGAR.

Purpose: The objective of this study was to investigate the efficacy of a siRNA-*tigar*-biopolymer, TI6752 (Tituxistatin), to therapeutically inhibit tumorigenesis in an in vivo xenograft model of colorectal cancer.

Materials and Methods: The overexpression of TIGAR within K-Ras+ tumor cells and the infiltration of PECAM-1+ endothelial progenitors in primary colorectal carcinoma clinical samples were detected by immunoconfocal microscopy. Immunodeficient NIH III-nude mice were subcutaneously engrafted with HCT116 colon cancer cells and then treated with three doses of TI6752 (1 mg/kg bw) or a Vehicle control, administered intravenously at weekly intervals. The animals were humanely sacrificed and HCT116 cells within the tumor tissues were visualized using an Anti-human Ki67 primary antibody. The accumulation of biotin-labeled TI6752 within preexisting HCT116 tumor tissues, compared to other secondary organs (heart, liver, kidneys), was visualized using an AlexaFluor488-conjugated Anti-Biotin primary antibody.

Results: We have shown that TIGAR is highly expressed in K-Ras+ colorectal carcinoma clinical samples and correlates with robust angiogenesis. Using a preclinical HCT116 xenograft model of colorectal carcinoma, we have demonstrated that therapeutic IV-administration of a pegylated siRNA-biopolymer, TI6752, inhibited tumor growth and reduced the infiltration of PECAM-1+ endothelial progenitors into xenograft tumor tissues without causing any adverse secondary effects.

Conclusion: This study has demonstrated that IV-delivery of a pegylated siRNA-biopolymer, TI6752, targeted against *tigar* mRNA transcripts, effectively inhibited tumor growth and angiogenesis in an HCT116 xenograft model of colorectal carcinoma. TI6752 could represent a effective therapeutic approach to target TIGAR's pro-oncogenic functions in human cancers.

Plain Language Summary: The TIGAR protein is upregulated in many human cancers and has been shown to confer a protective pro-survival advantage to tumor cells associated with aggressive cell proliferation, invasiveness/metastasis, and refractory therapy-resistance that often correlates with poor clinical prognoses. Nevertheless, its significant structural homology to a metabolic enzyme (fructose-6-phosphokinase/fructose-2,6-bisphosphatase) required for cellular energy production suggests the TIGAR protein may be an undruggable anti-oncological target. This recent era has highlighted the expanding applications of RNA therapeutics and, therefore, we have tested the efficacy of a siRNA-based biopolymer, TI6752, that inhibits *tigar* gene expression in an in vivo preclinical HCT116 xenograft model of

Received: 1 July 2025
Accepted: 26 October 2025
Published: 4 November 2025

colorectal cancer. These translational studies revealed that IV-administration of TI6752 prevented the growth of HCT116 colorectal carcinoma tumors in treated experimental animals without causing any observed adverse secondary effects. We also demonstrated that biotin-labeled TI6752 accumulated within the tumor parenchyma but was not detectable in other tissues, including the heart or liver. Our findings indicate that TI6752 could represent an effective approach to therapeutically target the expression and pro-oncogenic functions of TIGAR in refractory cancers that do not otherwise respond to conventional anticancer therapies.

Keywords: TIGAR, RNA interference therapy, anti-oncological, K-Ras, angiogenesis, colorectal cancer

Introduction

It is widely recognized that oncogene-addicted proliferating cancer cells require increased energy generation and ATP synthesis associated with enhanced glucose uptake and mitochondrial activity which can lead to the accumulation of toxic metabolic byproducts, including free radicals and reactive oxygen species (ROS).[1–5] Indeed, the oncogenic dysregulation of c-Myc induces p53 expression and causes oxidative DNA-damage that can contribute to genomic instability and cellular transformation as well as neoplastic disease progression.[6,7] The unscheduled activation of cellular oncogenes, such as *c-myc* or *k-ras*, can also cause transcriptional and DNA replication stress, due to oxidative genotoxicity and the depletion of nucleotides, which physiologically can result in chromosomal instability, cellular senescence and apoptosis.[8–14] Lin et al have demonstrated that elevated c-Myc expression leads to global transcriptional amplification and increased occupancy of the promoters of actively transcribed c-Myc target genes in tumor cells.[15] The TIGAR protein is a fructose-2,6-bisphosphatase which has been shown to translocate to the outer membranes of mitochondria and suppress the accumulation of damaging oncogene-induced ROS by increasing the intracellular levels of NADPH and reduced glutathione.[16–18] TIGAR reprograms cellular metabolism by inhibiting glycolysis and shifting cells toward the pentose phosphate pathway (PPP) and thereby promotes nucleotide biogenesis through the production of ribose-5-phosphate.[16] The c-Myc oncoprotein induces the expression of TIGAR which has been shown to protect tumor cells against oncogene-induced mitochondrial ROS and oxidative DNA-damage.[19–24] Intriguingly, however, Cheung et al have demonstrated that TIGAR does not inhibit the production of Rac1-induced proliferative ROS in response to c-Myc-activation and Wnt-signaling in intestinal adenoma tumor cells.[20] The translocation of TIGAR from the cytoplasm to the outer membranes of mitochondria occurs under conditions of hypoxia or glucose starvation and is dependent upon the activation of hypoxia-inducible factor-1 alpha (HIF-1a) and molecular interactions with hexokinase-2 (HK2).[17] Moreover, certain oncogenic viruses (the human T-cell lymphotropic virus type-1, HTLV-1, and high-risk human papillomaviruses, HPVs) have been shown to activate cellular kinases and induce serine-phosphorylation of the TIGAR protein associated with its hypoxia-independent mitochondrial targeting which promotes their cooperation with cellular oncogenes during viral carcinogenesis.[21–24] Nuclear localization of the TIGAR protein has also been demonstrated to stimulate the expression of nuclear receptor binding SET domain protein-2 (NSD2) through molecular interactions with the antioxidant regulator, NRF2, associated with increased epigenetic gene regulation by dimethylated K36-histone H3 (H3K36me2) and therapy-resistance in cancer cells.[25] TIGAR has also been shown to contribute to DNA-damage repair and could alleviate oncogene-associated transcriptional and replication stress by promoting nucleotide biogenesis through the PPP in tumor cells.[26] These finding collectively highlight the potential significance of TIGAR as a candidate target for anticancer therapy.

The TIGAR protein is upregulated in wild-type *TP53*+ and *TP53*-null colorectal carcinoma cell-lines and has been shown to contribute to intestinal regeneration and the development of colorectal carcinomas.[19] Knockout mice lacking *TIGAR* expression developed normally through adulthood and exhibited a reduced incidence of cancer, although these animals were partially impaired for intestinal regeneration and enteric tissue repair following injury by irradiation.[19] Furthermore, a transgenic model of colorectal adenoma in mice that were deficient for *APC* expression and also null for *TIGAR* exhibited a reduced incidence of tumor development and had normal intestinal crypt morphologies.[19] These findings suggest that TIGAR suppresses the accumulation of damaging ROS in proliferating tumor cells and contributes to the establishment and progression of colorectal carcinomas. Intriguingly, Keller et al have shown that stromal carcinoma-associated fibroblasts (CAFs) undergo a reverse-Warburg effect as they switch to aerobic glycolysis and produce ROS which supports the proliferation of colorectal carcinoma cells associated with enhanced metabolic activity and upregulation of TIGAR within the tumor cells.[27] Ahmad et al have reported that the surface glycoprotein, mucin 1 (MUC-1), which is overexpressed in many

colorectal cancers and correlates with tumor cell invasiveness, metastasis, and poor prognoses, regulates protein synthesis and the translation of TIGAR through the phosphatidylinositol-3-kinase (PI3K)/AKT and mammalian target of rapamycin complex 1 (mTORC1)/S6K1 pathways.[28] An inhibitory molecule, GO-203, which targets the MUC1-C subunit and prevents its oligomerization, inhibited the phosphorylation of AKT and blocked the eIF4A-dependent translation of TIGAR in two colon cancer cell-lines, SKC0-1 and Colo-205. Also, the repeated intraperitoneal administration of GO-203 daily for 28 days, or intravenously for 5 days per week for two weeks, caused the regression of Colo-205 and SKC0-1 xenograft tumors in treated BALB/c nude female mice.[28]

The TIGAR protein is upregulated in many types of cancers, including colorectal, prostate, gastric, esophageal, cervical, and non-small cell lung cancers, hepatocellular carcinoma, nasopharyngeal carcinoma, malignant glioma, multiple myeloma, adult T-cell leukemia/lymphoma (ATLL), acute lymphoblastic leukemia (ALL), and acute myeloid leukemia, and has been shown to correlate with therapy-resistance and is often an indicator of aggressive tumor cell proliferation and poor clinical outcomes.[19,21–24,29–44] Using a mesenchymal-specific *tigar* knockout mouse model, Wang et al demonstrated that TIGAR interacts with transforming growth factor beta-activated kinase-1 (TAK1) and enhances its ubiquitination by tumor necrosis factor receptor-associated factor-6 (TRAF6) and auto-phosphorylation, associated with NF-kB activation and pro-inflammatory cytokine receptor signaling in macrophages.[45] A pharmacological inhibitor of TAK1, 5Z-7-OX, sterically blocked the interaction of TIGAR with TAK1 and inhibited TIGAR-associated pro-inflammatory signaling in vitro and countered cecal ligation puncture-induced sepsis in 5Z-7-OX-treated animals.[45] The overexpression of p53 in combination with cisplatin chemotherapy treatment has been shown to result in decreased TIGAR protein levels and the sensitization of A549 lung cancer cells to cisplatin-induced DNA-damage and apoptosis.[46] Moreover, we have previously demonstrated that lentiviral-siRNA-inhibition of TIGAR expression inhibited tumorigenesis and tumor cell metastasis in murine xenograft models of HTLV-1-induced T-cell lymphoma and HPV-induced cervical carcinoma; and the siRNA-knockdown of TIGAR protein expression hypersensitized transfected HeLa (HPV18+) cervical cancer cells to oxidative DNA-damage and apoptosis caused by subinhibitory concentrations of the chemotherapy drugs, etoposide, doxorubicin, cisplatin, and 4-hydroxycyclophosphamide, suggesting the upregulation of TIGAR confers a protective pro-survival advantage to cancer cells which contributes to intractable therapy-resistance.[21–23,39] Thus, with the present study we sought to develop a translational strategy to therapeutically inhibit TIGAR's pro-oncogenic functions in an in vivo xenograft model of colorectal carcinoma using a pegylated siRNA-based biopolymer, TI6752.

Materials and Methods

Structural Comparison of the TIGAR and Fructose-6-Phosphokinase/Fructose-2,6-Bisphosphatase Proteins

The human TIGAR (NCBI MMDB ID: 65515) and fructose-6-phosphokinase/fructose-2,6-bisphosphatase (NCBI MMDB ID: 170720) protein structures were modeled and rendered using the UCSF-Chimera algorithm.[47] Structural comparisons were performed by generating a merged superimposed image of the folded protein structures using the UCSF-Chimera Matchmaker tool.

Immunoanalysis of Primary Colorectal Cancer Clinical Samples

TIGAR protein expression was detected within the K-Ras-positive tumor cells in a panel of de-identified, primary human colorectal adenocarcinoma clinical samples collected with a waiver of consent and provided by the Pathology Core Laboratory of the University of Hawaii Cancer Center. Some of the formalin-fixed paraffin-embedded (FFPE) colorectal carcinoma tissue sections were stained with hematoxylin and eosin (H&E) for anatomical analysis by microscopy. To detect the TIGAR protein within K-Ras+ colorectal cancer tumor cells, the tissue sections were deparaffinized by treatment with xylene for 3 min at room temperature with gentle agitation, followed by a 1:1 solution of xylene/ethanol for 3 min, and 2 x treatments with 100% ethanol for 3 min, 70% ethanol for 3 min, 50% ethanol for 3 min, and rinsed 2 x with distilled deionized water. The samples were incubated in a Microscopy Fixative solution (2% formaldehyde and 0.2% glutaraldehyde in phosphate buffered saline, PBS, pH 7.4) for 15 min at room temp and then rinsed 3 x with PBS, pH 7.4, and incubated in Blocking Buffer (3% w/v bovine serum albumin and 0.5% Tween-20 in PBS, pH 7.4) for 1 hr

on an orbital shaker. The samples were subsequently immunostained with a rabbit polyclonal Anti-TIGAR primary antibody (M-209; Santa Cruz Biotechnology, Dallas, TX) and mouse monoclonal Anti-K-Ras (3B10-2F2; Millipore-Sigma, St Louis, MO) primary antibody, diluted 1:1000 in BLOTTO Buffer (50 mM Tris-HCl, pH 8.0, 0.2 mM $CaCl_2$, 80 mM NaCl, 0.2% IGEPAL-CA630, 0.02% w/v sodium azide) for 2 hrs with gentle agitation. Next, the samples were washed 2x with BLOTTO buffer for 10 min and stained with rhodamine (TRITC)-conjugated AffiniPure donkey Anti-Rabbit IgG (H+L) and AlexaFluor Dylight 488-conjugated AffiniPure Donkey Anti-Mouse fluorescent secondary antibodies (diluted 1:500 in BLOTTO Buffer; Jackson Immunoresearch Laboratories, West Grove, PA) with 4'6-diamidino-2-phenyl-indole (DAPI; Invitrogen, Waltham, MA) for 1.5 hrs on an orbital shaker. Alternatively, the samples were immunostained with a mouse monoclonal Anti-CD31/Platelet endothlial cell adhesion molecule-1 (PECAM-1) primary antibody (H-3, Santa Cruz Biotechnology; diluted 1:1000 in BLOTTO Buffer) and a AlexaFluor Dylight 488-conjugated AffiniPure Donkey Anti-Mouse IgG (H+L) fluorescent secondary antibody to detect infiltrating CD31/PECAM-1+ endothlial progenitor cells. The samples were washed 2x with BLOTTO buffer for 10 min and once with PBS. pH 7.4 for 10 min, and then fluorescence mounting medium (Kirkegaard & Perry Laboratories, Gaithersburg, MD) and glass coverslips were added and the tissue sections were analyzed by immunofluorescence-confocal microscopy.

In vivo Xenograft Studies of Colorectal Carcinogenesis and Efficacy Testing of the Therapeutic siRNA-Biopolymer TI6752

For the in vivo xenograft studies of colorectal carcinoma tumorigenesis, immunodeficient NIH III-nude mice (*Crl:NIH-Lystb$^{g\text{-}J}$ Foxn1^{nu} Btk^{xid}*; Charles River Laboratories, Shrewsbury, MA), between 6–10 months of age and with equal numbers of male and female animals (n =8 per sample group), were anesthetized by inhalation of 3–5% isoflurane/O_2 using a Surgivet model 100 key-lock vaporizer (Harvard Apparatus Holliston, MA) with an induction chamber and small rodent nose cone and then subcutaneously engrafted over each hind flank with 7.5×10^5 HCT116 colorectal carcinoma cells (HD PAR-007; Horizon Discovery LTD, Cambridge, United Kingdom), diluted in 250 mL of the sterile Vehicle (Ca^{2+}/Mg^{2+}-free, PBS, pH 7.4), using a sterile 27-gauge tuberculin syringe. The animals were allowed to recover on a heated 37° C circulating water pad before they were returned to pathogen-free NexGen IVC rodent cage housing (Allentown LLC, Allentown, NJ). The animals were monitored daily for signs of tumor development or other changes to their overall health status (lethargy or other signs of morbidity, difficulty eating, drinking, or with proper ambulation). After 2 weeks, small tumor masses of at least 2 mm dia were visible in 100% of the engrafted animals. Then, the experimental animals were anesthetized and treated at weekly intervals with three doses of the pegylated siRNA-biopolymer TI6752 (1 mg/kg bw) dissolved in 200 mL of the sterile Vehicle, administered intravenously (by tail vein injections), using a sterile 31-gauge insulin syringe (BD Biosciences, Franklin Lakes, NJ). The pegylated siRNA-*tigar* biopolymer TI6752 was designed and complexed by the Harrod Laboratory (Southern Methodist University, Dallas, TX), dissolved in the sterile vehicle, and filter-sterilized by passage through a 4 mm (0.2 mm pore size) regenerated cellulose membrane syringe filter (Corning, Glendale, AZ) prior to injection in experimental animals. Another group of HCT116-engrafted animals was injected with the sterile Vehicle alone for comparison. Unengrafted (Control) animals were included as a negative control. The animals were monitored daily for signs of tumor growth or other changes to their overall health status. No animals were allowed to develop tumors >2 cm dia or exhibit signs of necrosis, and any animals in these categories were humanely euthanized to prevent unnecessary pain or suffering per the SMU institutional tumor burden policy. Only animals that completed the full 3-dose treatment schedule were included in the final data analysis. After a period of 5-weeks, the experimental animals were humanely sacrificed by inhalation of 70% CO_2 with cervical dislocation as a secondary physical measure to ensure death. Then, necropsies were performed to harvest the primary tumor masses which were weighed with a Mettler Toledo XP26 microanalytical balance (Thermo Fisher Scientific, Waltham, MA) and measured using a digital caliper to calculate their volumes using the formula $(D \times d^2)/2$, where "D" equals the longest diameter and "d" equals the shortest diameter. The tumor tissues were processed and fixed in 15x volumes of 10% neutral-buffered formalin (3.75% formaldehyde, 33.3 mM sodium phosphate monobasic, 45.8 mM sodium phosphate dibasic in distilled deionized water, pH 6.8) at room temp. The tissues were rehydrated by incubation in 50x volumes of 70% ethanol for 1 hr, 95% ethanol for 1.5 hrs, 100% ethanol for 1.5 hrs, and xylene for 1 hr with

gentle agitation and then embedded in Histoplast IM paraffin (Thermo Fisher Scientific) using Fisher Tissue Path IV cassettes and a Thermo Histostar tissue embedding system. Thin sections (0.5 mm) were prepared by cutting the paraffin-embedded tumor (or secondary organ) tissue blocks using a Microm HM360 rotary microtome (Carl Zeiss Microimaging, Oberkochen, Germany) and the samples were floated onto glass microscope slides, dried, and stored at −80° C until ready for analysis and imaging by immunoconfocal microscopy.

TI6752 is an experimental therapeutic and its chemical structure and method of synthesis are proprietary technologies that will be provided upon reasonable request through a consulting or other technology licensing agreement consistent with the Intellectual Property and Technology Management Policies of Southern Methodist University.

Immundetection of Human Ki67-Positive HCT116 Colon Cancer Cells and Infiltrating Endothelial Progenitors in Xenograft Tumor Tissues

The tumor tissue sections for the HCT116/TI6752-treated and HCT116/Vehicle control animals were deparaffinized, fixed, and incubated in Blocking buffer for 1 hr as described above and then immunostained using rabbit polyclonal Anti-Human Ki67 (H-300, Santa Cruz Biotechnology) or mouse monoclonal Anti-PECAM-1 (H-3; Santa Cruz Biotechnology) primary antibodies, diluted 1:1000 in BLOTTO Buffer, for 2 hrs at room temp on an orbital shaker. The samples were then washed 2 x with BLOTTO Buffer for 10 min and immunostained with Rhodamine red (TRITC)-conjugated AffiniPure Goat Anti-Rabbit IgG (H+L) or AlexaFluor Dylight 488-conjugated AffiniPure Donkey Anti-Mouse IgG (H+L) fluorescent secondary antibodies (Jackson Immunoresearch Laboratories), diluted 1:500 in BLOTTO Buffer for 1.5 hrs. The samples were then washed 2x with BLOTTO Buffer and once with PBS, pH 7.4 for 10 min each with gentle agitation, mounting medium and coverslips were added, and the tumor tissue sections were analyzed by immunofluorescence-confocal microscopy. The numbers of CD31/PECAM-1+ endothelial cells per field were quantified by counting triplicate visual fields for each sample at 200x magnification.

Intratumoral Accumulation of the Biotin-Labeled siRNA-Biopolymer TI6752 in IV-Treated HCT116-Engrafted Experimental Animals

To determine whether the intravenously administered siRNA-biopolymer TI6752 accumulates within tumor tissues and/or secondary organs, immunodeficient NIH III-nude mice (n =3 per sample group) were subcutaneously engrafted over each hind flank with 7.5×10^5 HCT116 colorectal carcinoma cells, diluted in 250 mL of the Vehicle, and the animals were monitored daily until moderately sized tumor masses were visible at the injection sites. Then, the animals were treated on consecutive days by IV-administration (tail vein injections) of the pegylated biotin-labeled siRNA-biopolymer, TI6752, diluted in 200 mL of the Vehicle. The biotinylated TI6752 siRNA-biopolymer contains a biotin chemical tag on the 3′ terminal cytosine of the siRNA-*tigar* nucleotide sequence. As a negative control, another group of animals was treated with the Vehicle alone for comparison. The animals were humanely sacrificed by 70% CO_2 inhalation and cervical dislocation within 6 hrs following the second injection of biotinylated TI6752 or the Vehicle control. The tumor tissues and secondary organs: heart, liver, and kidneys, were harvested, fixed in a 10% neutral-buffered formalin solution, paraffin-embedded and tissue sections were prepared as described for immunoanalysis by confocal imaging. The tissue sections were immunostained with an AlexaFluor Dylight 488-conjugated mouse monoclonal Anti-Biotin antibody (Jackson Immunoresearch Laboratories), diluted 1:250 in BLOTTO Buffer with DAPI nuclear stain included and incubated for 2 hrs at room temperature with gentle agitation. The samples were then washed 2 x with BLOTTO Buffer and PBS, pH 7.4, for 10 min each on an orbital shaker and analyzed by immunoconfocal microscopy.

Microscopy

The H&E-stained primary colorectal carcinoma tissues sections were imaged using a Zeiss Axioimager Z2 microscope with a MRc color camera and Plan Apochromat 10x/0.3 or Plan-Apochromat 20x/0.8 objectives and 10x ocular lenses (Carl Zeiss Microimaging). The excised HCT116 xenograft tumor masses were imaged on a Zeiss Discovery V8 stereomicroscope using a Plan Apo S 1.0x/FWD 60 mm objective (Carl Zeiss Microimaging). All immunofluorescence-confocal microscopy was performed on a Zeiss LSM800 confocal imaging system with a Plan Apochromat 20x/0.8

objective and 10x ocular lenses. 2.5D quantitation of the fluorescence micrographs for the biotinylated siRNA-biopolymer TI6752 and Vehicle (antibody control) samples was performed using the Carl Zeiss Microimaging ZEN OS 2.5D post-acquisition analysis tool.

Statistics

The numbers of experimental animals in each sample group (n =8) for the in vivo tumorigenesis and efficacy testing of the therapeutic pegylated siRNA-biopolymer TI6752 were determined using NCSS PASS sample-size statistical software (NCSS Statistical Software, Kaysville, UT) and calculated to have a power of 0.84479 (alpha = 0.050), which allows for a sample dropout rate of 20%. Graphed data represents the averages of the experimental data and the error bars indicate standard deviation between the samples. The statistical significance of the dataset for the quantitation of infiltrating CD31/PECAM-1+ endothelial progenitors per field in the HCT16 xenograft tumor tissues (n =5 with triplicate fields for each sample) was determined by one-way ANOVA (alpha =0.050; ****p-value <0.0001) using GraphPad Prism 8,0 software (GraphPad Software, Boston, MA).

Results

The Human TIGAR Protein Shares Structural and Sequence Homology with the Bifunctional Enzyme, Fructose-6-Phosphokinase/Fructose-2,6-Bisphosphatase

The primary amino acid sequence and structure of the human TIGAR protein are nearly identical to the C-terminal phosphatase domain of the bifunctional enzyme, fructose-6-phosphokinase/fructose-2,6-bisphosphatase, which has likely impeded the development of small-molecule pharmacological inhibitors of this key pro-oncogenic factor. We generated a space-filling model of the human TIGAR protein, complexed with a phosphate ion (MMDB ID: 65515), using the UCSF-Chimera algorithm (Figure 1A).[47] The TIGAR protein contains six helical domains and nine beta sheets connected by disordered random coils (Figure 1B, right panel). Also, the structure of the human fructose-6-phosphokinase/fructose-2,6-bisphosphatase protein (NCBI MMDB ID: 65515), with a bound N-aryl 6-aminoquinoxaline inhibitor 4,[48] was rendered and modeled using UCSF-Chimera (Figure 1B, left panel). We then used the UCSF-Chimera Matchmaker tool to generate a superimposed alignment of the folded structures of the TIGAR and fructose-6-PK/F-2,6-bisphosphatase proteins to compare their similarities (Figure 1C). As shown in Figure 1C, the TIGAR protein (in beige) exhibits nearly identical structural overlap with the C-terminus of the Fructose-6-PK/bisphosphatase protein (in blue) predicting it would be difficult to design a small molecule therapeutic that selectively inhibits TIGAR without also affecting this other metabolic regulator of glucose catabolism.

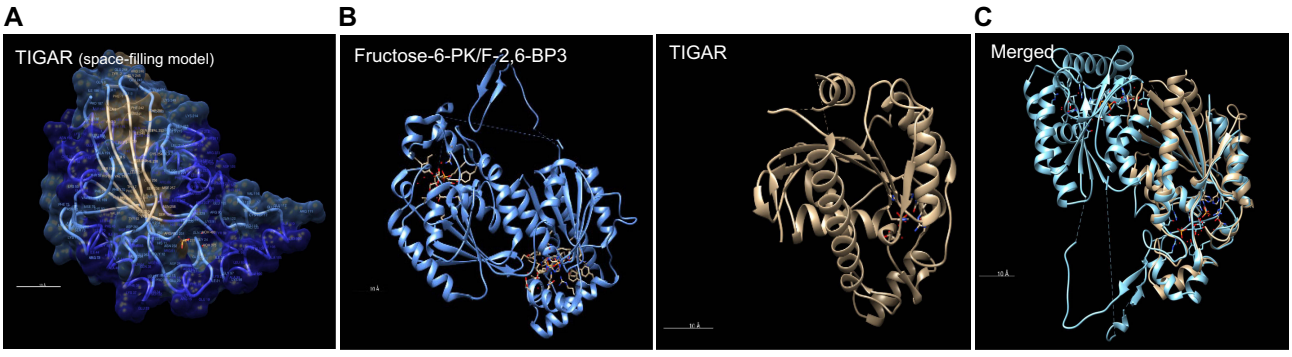

Figure 1 The TIGAR protein is structurally similar to the C-terminal phosphatase subunit of the bifunctional enzyme, fructose-6-phosphate, 2-kinase/fructose-2,6-bisphosphatase. (**A**) Space-filling model of the TIGAR protein structure (NCBI MMDB ID: 65515) with its secondary structures indicated (alpha helices, dark blue; coils, light blue; and sheets, beige). (**B**) The structures of the human fructose-6-PK/F-2,6,-bisphosphatase (NCBI MMDB ID: 170720; blue, left panel) and TIGAR (beige, right panel) proteins were modeled and rendered using the UCSF-Chimera algorithm. (**C**) Merged superimposed image of the fructose-6-PK/F-2,6-bisphosphatase (blue) and TIGAR (beige) protein structures generated using the UCSF-Chimera-Matchmaker comparison tool. Scale bar, 10 Angstroms (Å).

High Levels of TIGAR Correlate with the Recruitment of Stromal Endothelial Progenitors and Angiogenesis in Primary Colorectal Carcinoma Tissues

The TIGAR protein has been shown to be upregulated in human colorectal cancers which contained either wild-type or mutant TP53.[19] Using a transgenic *Tigar*$^{-/-}$ knockout mouse model as well as an inducible model of *adenomatous polyposis coli* (*APC*)-deletion-associated intestinal tumorigenesis, Cheung et al have demonstrated that TIGAR is required for intestinal regeneration following injury by irradiation or chemical intestinal ablation after repeated treatment with dextran sulfate sodium (DSS), as well as for intestinal tumorigenesis in vivo.[19] We therefore examined the expression of the TIGAR protein in a panel of biopsied, primary colorectal adenocarcinoma tissue samples provided by the Pathology Core Laboratory of the University of Hawaii Cancer Center. The micrographs of the H&E stained tissue sections show the invasive fronts and ductal morphology of these colorectal adenocarcinomas (Figure 2A and B, top panels). The expression of TIGAR within the K-Ras-positive tumor cells was visualized by immunofluorescence-confocal microscopy (Figure 2B, see insets). The COL-5 sample was also stained with non-specific rabbit immunoglobulin (IgG) as a negative antibody control (Figure 2C). Interestingly, we observed that the primary colorectal carcinoma clinical samples exhibited robust infiltration by CD31/Platelet endothelial cell adhesion molecule-1 (CD31/PECAM-1)-positive stromal endothelial progenitors associated with tumor angiogenesis that correlated with the upregulation of TIGAR (Figure 2B, middle panels). Consistent with these findings, Yapindi et al have previously reported that lentiviral siRNA-*tigar* knockdown of TIGAR expression in an in vivo HeLa xenograft model of HPV18-induced carcinogenesis resulted in tumors of diminished size with smooth borders that were poorly vascularized and lacked an invasive front.[23] These data suggest that the upregulation of TIGAR contributes to colorectal carcinogenesis as well as heterotypic signaling between the TIGAR/K-Ras-positive enteric epithelial tumor cells and mesenchymal endothelial stem cells to promote angiogenesis and malignant disease progression.

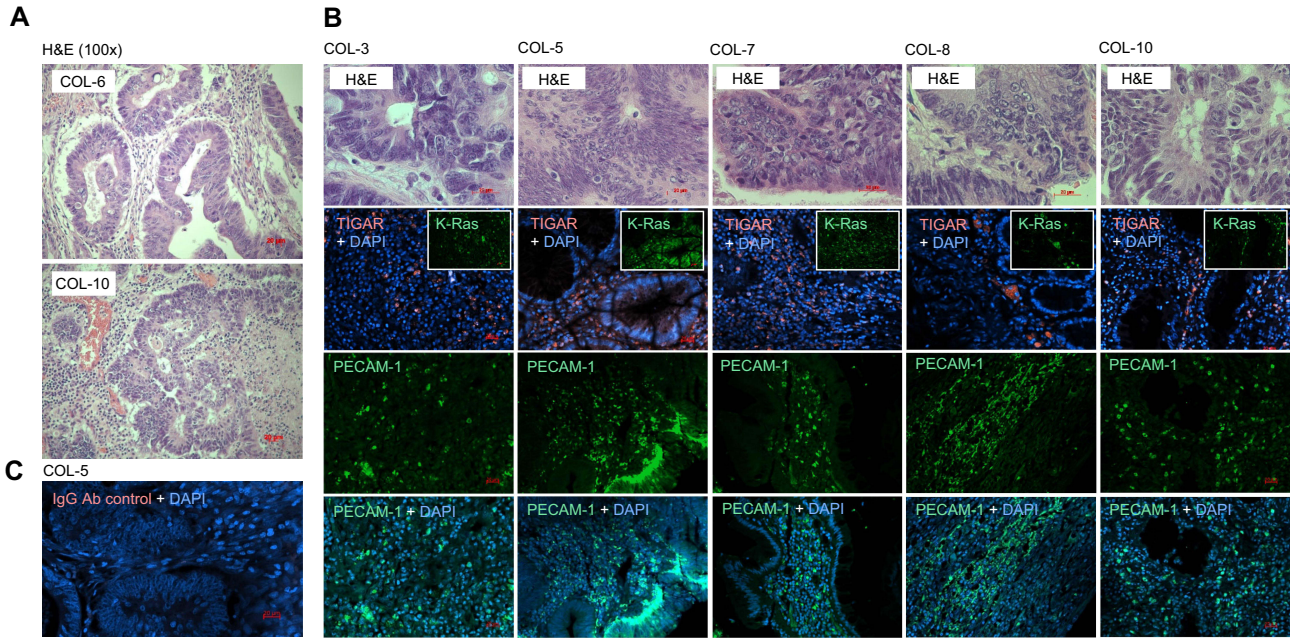

Figure 2 The TIGAR protein is highly expressed in K-Ras+ primary colorectal carcinoma clinical samples. (**A**) Representative FFPE colon cancer biopsy specimens were stained using hematoxylin and eosin (H&E) and kindly provided by the Pathology Core Laboratory of the University of Hawaii Cancer Center and then imaged at 100x magnification. (**B**) Primary colorectal carcinoma clinical samples were stained using H&E (top panels) or immunostained (bottom panels) using primary antibodies that recognize TIGAR (red signal), K-Ras (green signal, insets), or PECAM-1 (green signal) and appropriate fluorescent secondary antibodies (Jackson Immunoresearch Laboratories) and then imaged by immunoconfocal microscopy at 200x magnification. (**C**) Alternatively, the COL-5 tumor sample was immunostained using a non-specific rabbit IgG antibody control (red signal). DAPI nuclear staining (blue signal) is provided in merged images for reference. Scale bar, 20 mm.

https://doi.org/10.2147/JEP.S546622

Therapeutic Intravenous Administration of the siRNA-Biopolymer TI6752 Effectively Inhibited Tumor Growth in an in vivo HCT116 Xenograft Model of Colorectal Carcinogenesis

The HCT116 colorectal carcinoma cell-line induces aggressive tumor growth in engrafted immunodeficient NIH III-nude animals. We initially established the baseline kinetics of tumorigenesis to optimize experimental conditions by subcutaneously engrafting NIH III-nude mice with 1×10^6 HCT116 colorectal carcinoma cells, diluted in 250 mL of the sterile vehicle, using a 27-gauge tuberculin syringe. In parallel, another sample group was injected with the Vehicle alone as a negative control. As shown in Figure 3A and B, the animals injected with 1×10^6 HCT116 cells developed large xenograft tumor masses over

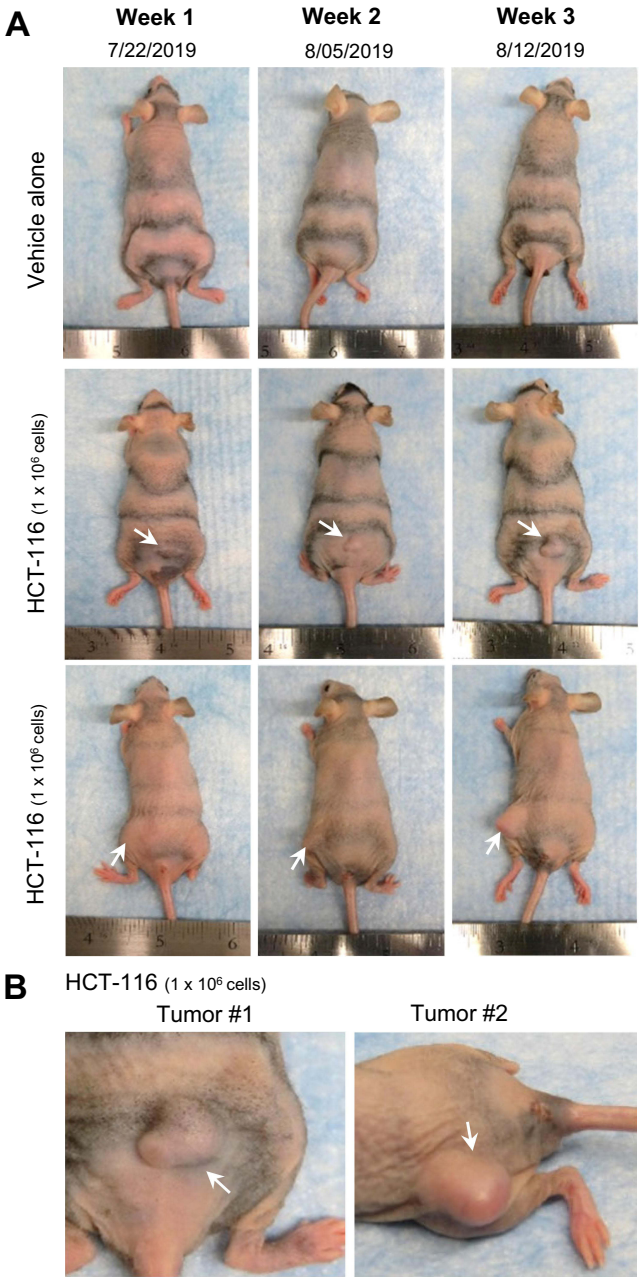

Figure 3 Time-course of tumor development and growth in immunodeficient NIH III-nude mice engrafted with the HCT116 colorectal carcinoma cell line. (**A**) To establish the baseline kinetics of tumorigenesis for our initial experimental optimization, NIH III-nude mice (n =3) were anesthetized and then subcutaneously engrafted with either the Vehicle alone (top panels) or 1×10^6 HCT116 colorectal carcinoma cells diluted in 250 mL of the sterile vehicle (data for two representative animals are shown in the lower panels). The animals were closely monitored over a three-week period for tumor development and growth (indicated by white arrows). (**B**) Enlarged images of the primary tumor masses (white arrows) formed by the end of the third week in two animals engrafted with HCT116 colorectal carcinoma cells.

a period of 3-weeks (indicated by arrows in the images). Next, to determine if the therapeutic inhibition of TIGAR expression could prevent the growth of colorectal carcinoma tumor cells in vivo and/or cause the regression of existing tumor masses, immunodeficient NIH III-nude mice were subcutaneously engrafted with the tumorigenic HCT116 colorectal carcinoma cell-line and monitored for the appearance of visible tumor masses of at least 2 mm dia at the site of injection. Another group of animals was injected with the Vehicle alone as a negative control. The HCT116-engrafted tumor-bearing animals were then anesthetized and treated with three doses (1 mg/kg bw) of a filter-sterilized pegylated siRNA-*tigar* biopolymer, TI6752 (Tituxistatin), delivered at 1-week intervals by intravenous (ie, tail vein) injections and the animals were monitored daily over a period of 5-weeks for signs of tumor growth or any other changes to their overall health status. As a control, a second group of HCT116-engrafted tumor-bearing animals were intravenously injected 3x at weekly intervals with the Vehicle alone for comparison. Surprisingly, as shown in Figure 4A and B, the HCT116/Vehicle animals exhibited aggressive tumor growth and developed large pronounced masses over a 5-week time-course, in contrast to the HCT116/TI6752-treated animals for which most did not exhibit a significant increase in tumor size beyond the existing 2 mm dia masses present at the time of initial treatment (Figure 4A and B, see arrows). Although the xenograft tumors in the HCT116/TI6752-treated animals remained static and without a significant increase in size, we did not observe any regression or further diminishment of tumor size in these animals –however, it is anticipated these masses would likely eventually regress over an extended period. None of the HCT116/TI6752-treated animals exhibited any adverse secondary effects (ie, weight loss, reduction in appetite/drinking, altered ambulation or attentiveness, signs of lethargy or morbidity) and all of these experimental animals appeared healthy – indicating the treatments were well tolerated. At the end of the experimental period, the animals were humanely euthanized and necropsies were performed, and the primary tumor masses (see arrows) were harvested, weighed, and measured using a digital caliper (Figure 4B, lower panels, C and D). The average tumor weights and volumes in the HCT116/TI6752-treated animals were markedly reduced as compared to the HCT116/Vehicle animals (Figure 4C and D), suggesting the inhibition of TIGAR by TI6752 could represent an effective therapeutic approach to target TIGAR's pro-oncogenic functions in human cancers. We have also provided representative time-course data for the tumor growth kinetics in two additional animals for the HCT116/Vehicle and HCT116/TI6752-treated sample groups, as well as an example of the Vehicle alone negative control in Figure 5, demonstrating that the TI6752-treated animals displayed markedly reduced tumorigenic growth compared to the HCT116/Vehicle experimental group (see arrows in the images).

Treatment with TI6752 Reduced the Infiltration of HCT116 Xenograft Tumor Tissues by Stromal PECAM-1+ Endothelial Progenitors and Inhibited Tumor Angiogenesis

As the primary colorectal carcinoma clinical isolates were found to contain significant numbers of infiltrating CD31/PECAM-1+ endothelial progenitors that correlated with high levels of TIGAR protein expression (Figure 2B), we next investigated whether the therapeutic inhibition of TIGAR might influence the chemotactic recruitment of endothelial stem cells into the tumor tissues of HCT116/TI6752-treated experimental animals versus the HCT116/Vehicle control. Formalin-fixed paraffin-embedded tissues sections were prepared and immunostained using primary antibodies against human Ki67 (Hu-Ki67) and CD31/PECAM-1 and appropriate fluorescent secondary antibodies, together with DAPI nuclear-staining for reference, and then the samples were analyzed by immunoconfocal microscopy. As a negative antibody control, one of the tumor sections was immunostained using non-specific rabbit IgG and a fluorescent rhodamine red (TRITC)-conjugated secondary antibody. The HCT116/TI6752-treated tumors were generally of smaller size and contained fewer huKi67-positive carcinoma cells than the tumor tissues from the HCT16/Vehicle control animals (Figure 6A). Importantly, there was a significant reduction in the recruitment of stromal murine CD31/PECAM-1-positive endothelial progenitors into the xenograft tumors of HCT116/TI6752-treated animals as compared to the HCT116/Vehicle control animals (Figure 6B); and these data are graphically presented in Figure 6C. These results are consistent with previous reports that elevated TIGAR expression correlates with enhanced tumor angiogenesis and vascularization in HPV+ uterine cervical cancers and HTLV-1+ T-cell lymphomas,[22,23] and further indicate that therapeutically targeting TIGAR can also block heterotypic signaling associated with angiogenesis and inhibit the growth of cancerous tumors via multiple mechanisms.

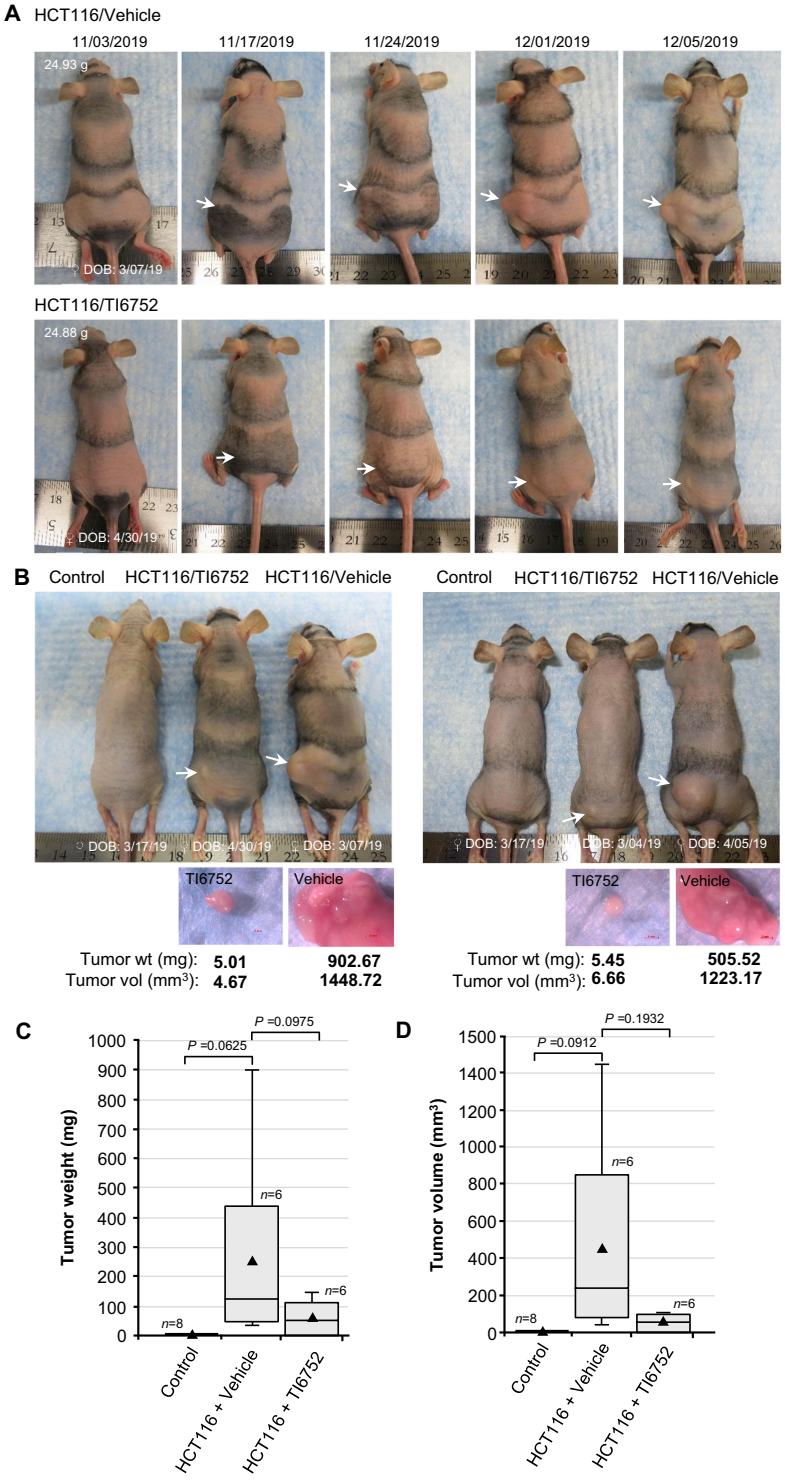

Figure 4 The pegylated siRNA-biopolymer TI6752 inhibits tumorigenesis in an in vivo xenograft model of colorectal carcinoma. (**A**) Time-course of tumor development in experimental NIH III-nude mice that were subcutaneously engrafted with HCT116 colorectal carcinoma cells and then treated with three doses of either TI6752 (1 mg/kg bw; bottom panels) or the Vehicle as a negative control (top panels), administered intravenously (by tail vein injections) at weekly intervals. The white arrows indicate the locations of primary tumor masses. (**B**) Two separate groups of experimental animals: Control (unengrafted), HCT116/TI6752-treated, HCT116/Vehicle control. The white arrows indicate the growth of large tumor masses in the HCT116/Vehicle control animals, as compared to HCT116/TI6752-treated mice. Tumors harvested from these experimental animals (lower panels) were weighed and then measured using a digital caliper to determine their volumes. Scale bar, 2 millimeters. The values of the weight and volume measurements are represented in bold type. (**C**) Graphed data of the average weights of tumor masses from the Control (sample size: n =8), TI6752/TI6752-treated, and HCT116/vehicle control (sample size: n =6) animals. (**D**) The relative volumes of tumors harvested from the experimental animals were calculated using the formula: $(D \times d^2)/2$, where "D" equals the longest diameter and "d" equals the shortest diameter. Error bars in C and D represent standard deviation between the samples. The statistical significance of the datasets was determined based upon their Student's *t*-distribution values in two-tailed unpaired tests (alpha =0.05) and calculated *p*-values using the Shapiro–Wilk normality test and Graphpad Prism 8.0 software.

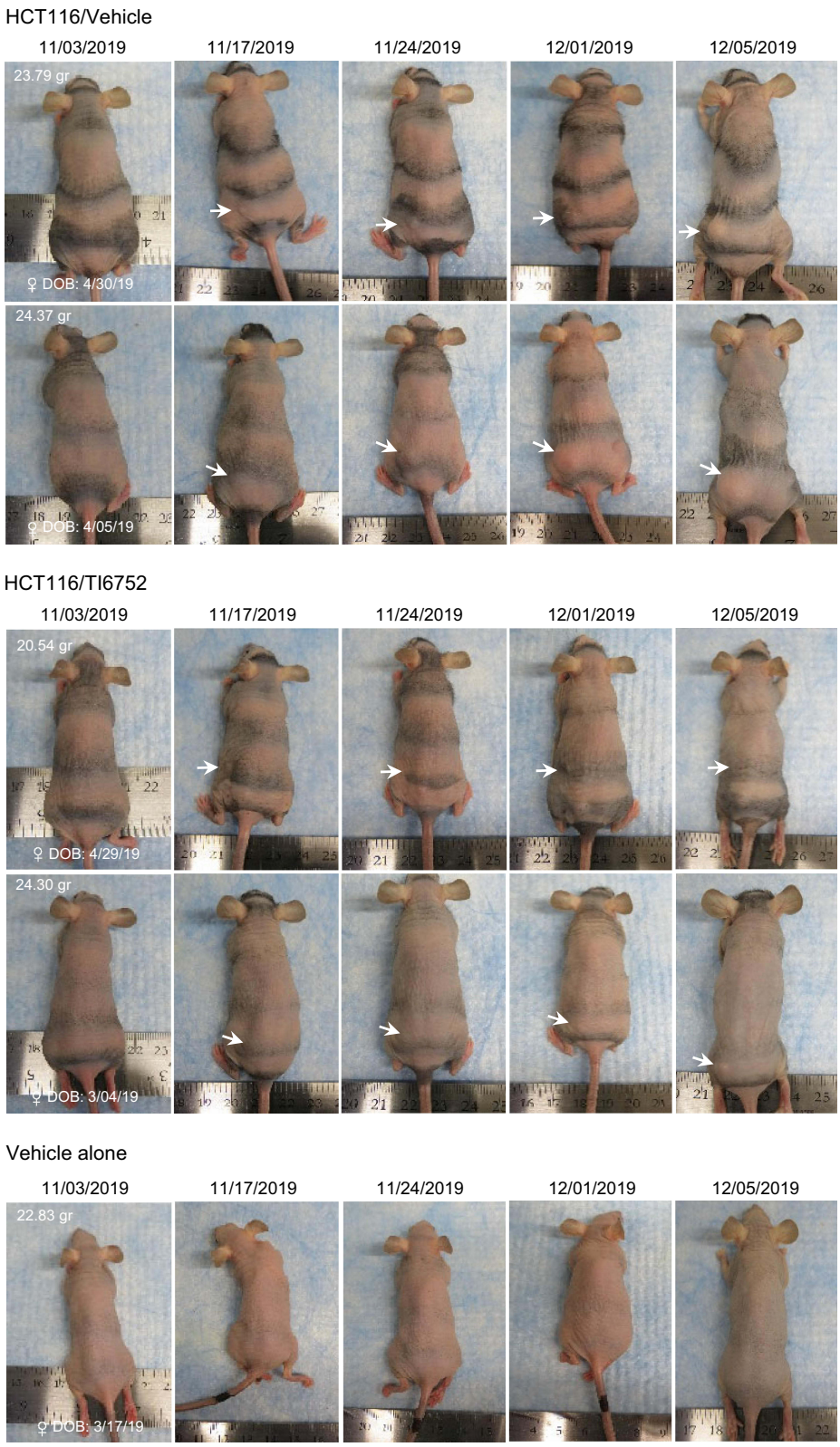

Figure 5 Comparative time-courses of HCT116 colorectal carcinoma tumor growth in representative experimental animals treated with the pegylated siRNA-biopolymer TI6752 or the Vehicle control. Immunodeficient NIH III-nude mice (n =6) were anesthetized and subcutaneously engrafted with the tumorigenic HCT116 colorectal carcinoma cell-line and then monitored until primary tumor masses of 2 mm dia were visible at the injection sites (indicated by the white arrows). The animals were subsequently treated with three doses of TI6752 (1 mg/kg bw; middle panels) or the Vehicle control (top panels), delivered intravenously, at weekly intervals. Another sample group was subcutaneously injected with the Vehicle alone as a negative control for comparison (bottom panels). Two representative animals are shown for the HCT116/Vehicle and HCT116/TI6752 experimental groups. The HCT116/Vehicle animals developed notably larger tumor masses than the HCT116/TI6752-treated animals by the end of the 5-week experimental period (see white arrows).

https://doi.org/10.2147/JEP.S546622

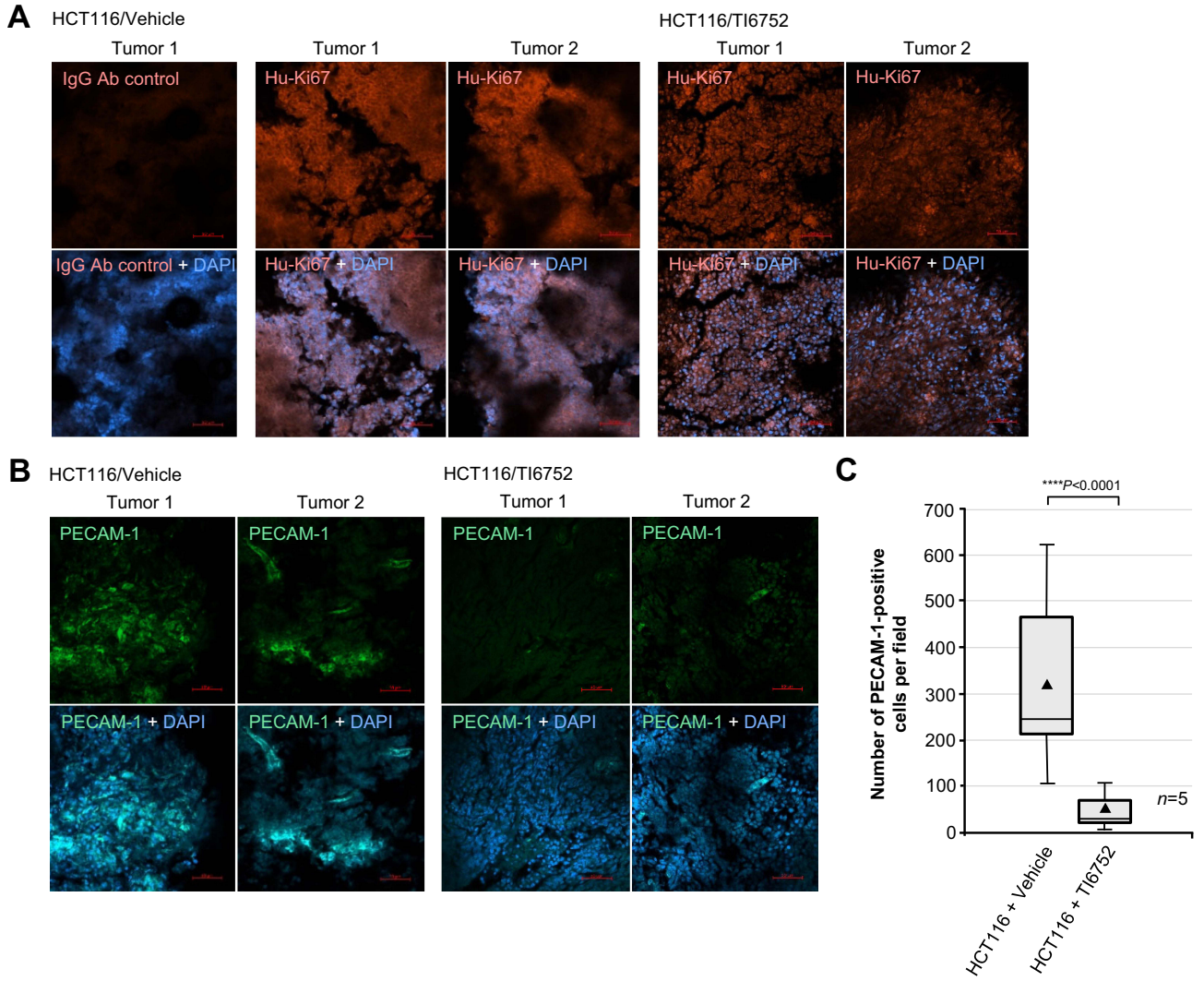

Figure 6 The inhibition of in vivo tumor growth by TI6752 correlated with reduced angiogenesis and infiltration by PECAM-1+ endothelial progenitors. (**A** and **B**) Immunoconfocal microscopy was performed to visualize HCT116 colorectal carcinoma cells (red signal) within the xenograft tumor tissues using an Anti-Human Ki67 primary antibody (in (**A**)), and the infiltration of PECAM-1+ endothelial stem cells (green signal) associated with tumor angiogenesis using an Anti-PECAM-1 antibody (in (**B**)). Two representative tumors are shown for the HCT116/Vehicle control (left panels) and HCT116/TI6752-treated animals (right panels). DAPI nuclear staining is provided in merged images for reference. Scale bar, 20 mm. (**C**) Graphical representation of the average numbers of PECAM-1+ endothelial progenitor cells per visual field at 200x magnification (n =5).The statistical significance of the datasets was determined based upon their Student's *t*-distribution values in two-tailed unpaired tests (alpha =0.05) and calculated *p*-values using the Shapiro–Wilk normality test and Graphpad Prism 8.0 software (**** $p < 0.0001$). Error bars represent standard deviation between the samples.

Accumulation of the Biotinylated RNA Therapeutic, TI6752, within HCT116 Xenograft Tumor Tissues but Not in Secondary Heart or Liver Tissues Following IV-Administration

Next, to determine if the pegylated siRNA-biopolymer TI6752 primarily targets HCT116 xenograft tumor tissues in vivo, immunodeficient NIH III-nude mice (n =3) were subcutaneously engrafted over each hind flank with the tumorigenic HCT116 colorectal carcinoma cell-line and monitored for the development of moderately sized tumor masses (see arrows in Figure 7A and C). The experimental animals were then anesthetized and treated on consecutive days with two doses of a biotin-labeled, pegylated siRNA-biopolymer TI6752 (1 mg/kg bw) administered by intravenous (tail vein) injections using a sterile 31-gauge insulin syringe. As a negative control, another group of HCT116-engrafted tumor-bearing animals was injected with the Vehicle alone. Within 6 hrs after the second treatment, the animals were humanely euthanized and necropsies were performed to harvest the HCT116 xenograft tumor masses and representative secondary

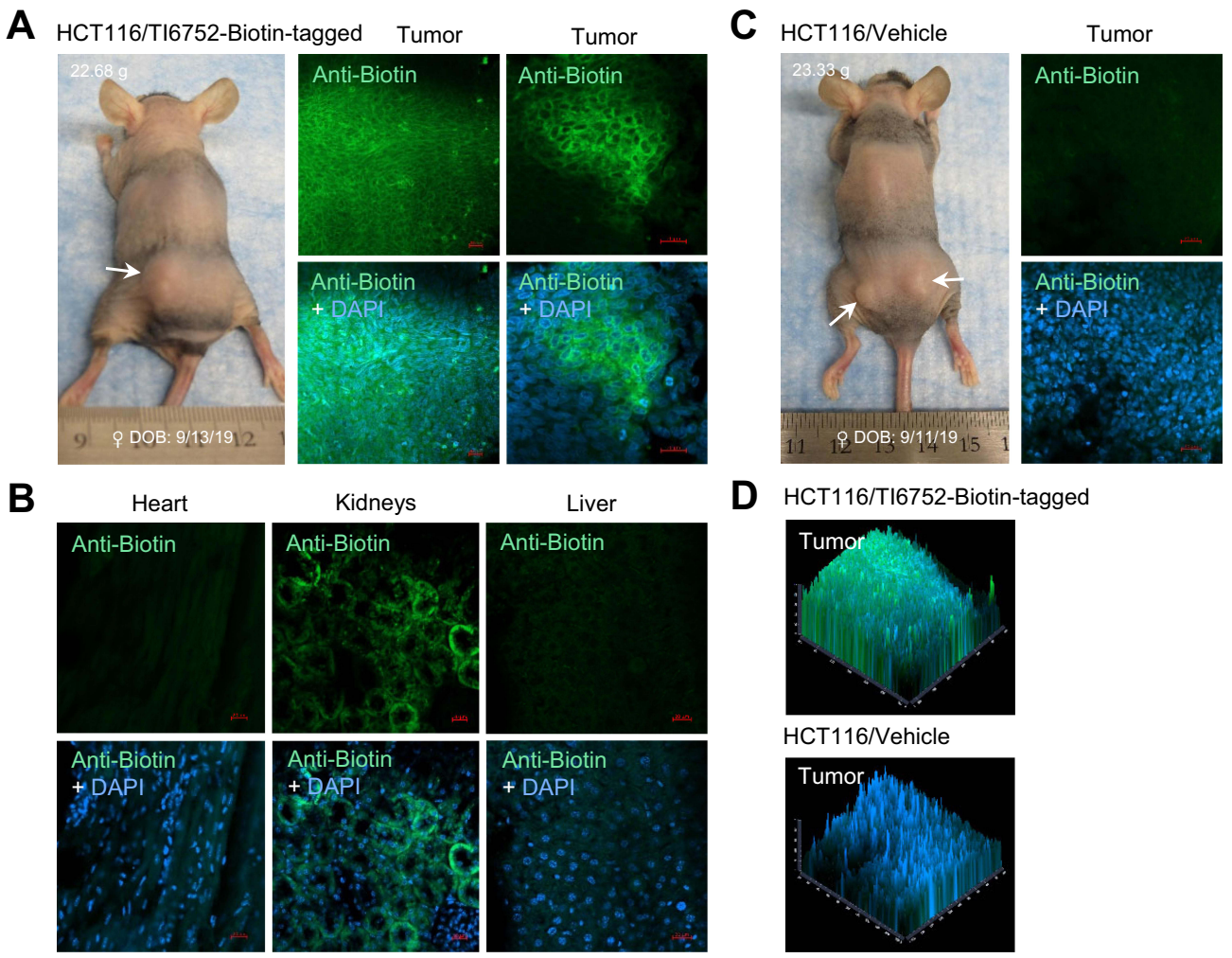

Figure 7 The biotin-labeled pegylated siRNA-biopolymer, TI6752, accumulates within HCT116 xenograft tumor tissues in vivo. (**A**–**C**) Engrafted NIH III-nude mice (n =3) with preexisting HCT116 tumors (arrows) were treated by IV-administration of the biotinylated siRNA-biopolymer TI6752, or a Vehicle control (in (**C**)), on two consecutive days and then the tumor tissues and secondary organs (heart, liver, kidneys) were analyzed by immunoconfocal microscopy using an Alexa Fluor 488-conjugated Anti-Biotin primary antibody (green signal). Scale bar, 20 mm. (**D**) 2.5-D quantitation of the Anti-Biotin 488 nm and DAPI fluorescent signals from micrographs of the HCT116/TI6752-biotin-tagged and HCT116/Vehicle control tissue samples using the Carl Zeiss Microimaging ZEN OS 2.5-D post-acquisition analysis tool.

organs (heart, liver, and kidneys). The FFPE tissue sections were subsequently analyzed by immunoconfocal microscopy using a fluorescent monoclonal Anti-Biotin antibody. As shown in Figure 7A–D, the biotinylated siRNA-biopolymer TI6752 significantly accumulated within the HCT116 tumor tissues and primarily localized in the cytoplasm of HCT116 carcinoma tumor cells (Figure 7A and D). DAPI nuclear-staining was included in the merged images to visualize the tumor cells as well as the surrounding murine stromal cells. The HCT116/Vehicle tumor tissues were immunostained as a specificity control for the fluorescent Anti-Biotin antibody (Figure 7C and D). Throughout this study, there was no significant toxicity or morbidity observed in TI6752-treated experimental animals and, consistent with this, the biotinylated siRNA-biopolymer TI6752 was not detected in the heart muscle or liver tissues of HCT116/TI6752 animals (Figure 7B, left and right panels). However, the biotin-labeled TI6752 was present within the tubular epithelial nephron structures of the kidneys likely associated with its renal excretion and clearance (Figure 7B, middle panels). Comparative graphical representations of the Anti-Biotin and DAPI fluorescent signals for the HCT116/TI6752-Biotin-tagged and HCT116/Vehicle tumor tissues were generated using the Carl Zeiss Microimaging ZEN OS 2.5D post-acquisition quantitation tool and are provided in Figure 7D.

https://doi.org/10.2147/JEP.S546622

Discussion

The TIGAR protein prevents the accumulation of damaging mitochondrial ROS and protects metabolically active proliferating cells against oncogene-induced oxidative damage through its antioxidant functions by increasing the intracellular levels of NADPH and reduced glutathione.[16–23] TIGAR has been shown to translocate from the cytoplasm to the outer membranes of mitochondria under conditions of hypoxia or glucose starvation which required the activation of HIF-1a and molecular interactions with HK2.[17] TIGAR also contributes to mitochondrial quality control and protects neuronal tissues against ischemic injury by inducing autophagy and the activation of Nrf2 antioxidant signaling.[49–51] Several studies have reported that TIGAR is upregulated in many types of cancers, including colorectal cancer, HPV+ cervical cancers, renal cell carcinoma, gastric cancers, hepatocellular carcinoma, ovarian cancer, nasopharyngeal carcinoma, prostate cancers, esophageal squamous cell carcinoma, malignant glioma, ATLL, ALL, AML, multiple myeloma, and non-small cell lung cancer, usually associated with aggressive proliferative disease phenotypes and poor clinical prognoses.[19,21–24,29–44] The in vitro knockdown of TIGAR expression has been shown to sensitize tumor cells to radiation and chemotherapeutic agents, suggesting TIGAR could be a key determinant of anticancer therapy-resistance.[34,35,39–43,52] However, the TIGAR protein shares extensive structural homology with the bifunctional, fructose-6-phosphokinase/fructose-2,6-bisphosphatase (Figure 1B and C), which has likely made it difficult to design specific pharmacological inhibitors of this candidate pro-oncological target for the treatment of human cancers. We have previously demonstrated that a synthetic siRNA-tigar oligonucleotide or lentiviral-siRNA-*tigar* could specifically inhibit TIGAR expression in vitro and in vivo in HTLV-1+ ATL tumor lymphoblasts and HPV+ cervical carcinoma cells and, therefore, we sought to generate a derivative of siRNA-*tigar* to facilitate its therapeutic delivery in vivo.[21–24] The present study demonstrated that a pegylated siRNA-biopolymer TI6752, targeted against *tigar* mRNA transcripts, inhibited tumor growth and angiogenesis in vivo in an HCT116 xenograft preclinical model of colorectal carcinoma without causing any adverse secondary toxicity in treated experimental animals. The TIGAR is an ideal candidate to therapeutically target using an RNA-based knockdown approach –since the TIGAR protein is induced in response to physiological stresses and frequently upregulated in cancer cells; and *tigar*$^{-/-}$ null transgenic KO mice were found to develop normally into adulthood and exhibited a reduced incidence of cancers,[19] suggesting TIGAR is redundant with F-6-PK/F-2,6-BFP and may be dispensable in most normal tissues.

We initially examined the expression of TIGAR in human colorectal cancers. Cheung et al have demonstrated that TIGAR is upregulated in colorectal carcinoma primary tumors as well as in the distal liver metastases.[19] Consistent with these findings, our results in Figure 2A–C revealed that the TIGAR protein is highly expressed within the K-Ras-positive tumor cells in a panel of primary colorectal carcinoma clinical isolates and correlated with robust angiogenesis and the infiltration of tumor tissues by stromal CD31/PECAM-1-positive endothelial progenitors (Figure 2B). Next, we investigated whether an siRNA-biopolymer, TI6752, targeted against *tigar* mRNA transcripts, could therapeutically inhibit tumorigenesis in an in vivo HCT116 xenograft model of colorectal carcinoma. The experimental animals were subcutaneously engrafted with HCT116 colorectal carcinoma cells and then monitored over a 2-week period until tumor growth of 2 mm dia was observed in 100% of the animals. Then the HCT116-engrafted animals were treated over the next 3 weeks by IV-administration of TI6752 or the Vehicle control and tumor growth was followed over a 5-week period. These studies revealed that tumor growth in the HCT116/TI6752-treated animals was significantly blocked as compared to the HCT16/Vehicle control animals which exhibited aggressive tumor development (Figures 4A–D and 5). Although the small tumors in the HCT116/TI6752-treated mice remained static and did not regress over the 5-week experimental period, we speculate these tumors would further diminish in size with additional treatments over an extended time. The appearance of these tumors in the HCT116/TI6752-treated animals was notably smooth and lacking an invasive front and almost devoid of microvessels (Figure 4B, lower panels). In agreement with these findings, the tumor tissues of the HCT116/TI6752-treated animals exhibited markedly diminished infiltration by CD31/PECAM-1-positive endothelial progenitors (Figure 6B and C), suggesting that inhibiting TIGAR also resulted in impaired angiogenic signaling and reduced tumor vascularization. The role of TIGAR in angiogenesis is complex and not well understood. He et al have reported that aortic endothelial cells derived from *tigar*$^{-/-}$ KO mice exhibit enhanced proliferation, migration, tube formation and sprouting ex vivo as a result of enhanced glycolytic functions.[53] Whereas, by contrast, Hennigs et al have demonstrated that TIGAR expression is induced as a component of a vasculoprotective

and regenerative endothelial program regulated by Peroxisome proliferator-activated receptor gamma (PPARg) and p53 in pulmonary arterial and lung microvascular endothelial cells in response to DNA damage or oxidative stress associated with pulmonary arterial hypertension (PAH).[54] Thus, the inhibition of TIGAR functions by TI6752 could interfere with chemoattractant signaling within HCT116 colorectal cancer tumor cells and diminish the recruitment of murine stromal endothelial stem cells, or, alternatively, TI6752 might impede angiogenic signaling within the endothelial progenitors and inhibit their migration and responsiveness to pro-angiogenic factors produced by the tumor cells. It is further possible the inhibition of TIGAR expression by TI6752 could inhibit TIGAR-induced pro-inflammatory signaling by interfering with TIGAR-TAK1 interactions and NF-kB activation which would be predicted to impact tumorigenesis as well as angiogenesis.[45]

The biotin-labeled TI6752 siRNA-biopolymer accumulated within the HCT116 xenograft tumor tissues of experimental animals following IV-administration but was not detected in the heart muscle or liver by immunoconfocal imaging using a fluorescent Anti-Biotin antibody (Figure 7A–D). It is well established that tumor capillaries are often leakier and have larger diameters than normal microvessels which can cause separations between their endothelial gap junctions; hence, we sought to exploit this characteristic property of cancer tissues for the intravenous delivery of TI6752 into the tumor parenchyma. Moreover, our earlier studies in Yapindi et al have demonstrated that siRNA-inhibition of TIGAR expression hypersensitized HPV18+ HeLa cervical carcinoma cells to oxidative DNA-damage and apoptosis induced by subinhibitory concentrations of the chemotherapeutic agents: doxorubicin, etoposide, cisplatin, and 4-hydroxycyclophosphamide.[39] These findings suggest that adjuvant therapy with a pharmacological inhibitor of TIGAR, in combination with other anticancer chemotherapeutics, might improve the efficacy of these drugs at lower dosages and, thus, reduce their secondary effects, such as cardiotoxicity or nephrotoxicity, to make them better tolerated in patients undergoing treatment.[55–59]

In addition to its potential anti-oncological role, TI6752 could have applications as an antiviral –since RNA viruses, such as filoviruses (Ebola and Marburg viruses), flaviviruses (Dengue virus), rhabdoviruses, coronaviruses, and influenza viruses, require ribose-5-phosphate produced via the PPP to support ribonucleotide biosynthesis for their replication and the expression of viral gene products. Indeed, the antiviral immune response to dsRNA activates Protein kinase RNA-activated (PKR) which phosphorylates and inhibits ribose 5-phosphate isomerase (RPIA) to reduce the intracellular levels of ribose-5-phosphate.[60] TIGAR drives the production of ribose-5-phosphate to promote nucleotide biosynthesis and, therefore, we speculate that therapeutically inhibiting TIGAR may represent a plausible countermeasure strategy to combat certain viral infections for which no antivirals currently exist. We and others have shown that TIGAR is highly expressed in HTLV-1- and HPV16/18-infected cells associated with viral carcinogenesis,[21–24,29,39] and it is likely the upregulation of TIGAR supports viral replication and mRNA transcription and enhances the survival and stress-tolerance of virus-infected cells through TIGAR's antioxidant and phosphatase functions during pathogenesis.

Conclusions

In conclusion, this study has demonstrated that an intravenously administered siRNA-biopolymer, TI6752, which targets *tigar* mRNA transcripts, effectively inhibited tumor growth and angiogenesis in a HCT116 xenograft model of colorectal carcinoma without causing adverse secondary effects. Biotinylated TI6752 accumulated within the HCT116 xenograft tumor tissues but not other organs, including the heart muscle or liver. The TIGAR protein structure is nearly identical to the C-terminal phosphatase subunit of the bifunctional, fructose-6-phosphokinase/fructose-2,6-bisphosphatase suggesting it may be difficult to specifically drug the functional domains of the TIGAR protein. Here, we have demonstrated that a pegylated RNA-based anti-oncological TI6752 inhibits tumorigenesis in vivo and could represent an effective translational strategy to therapeutically target TIGAR's pro-oncogenic functions in human cancers.

Abbreviations

ATP, adenosine triphosphate; DAPI, 4′,6-diamidino-2-phenylindole; FFPE, formalin-fixed paraffin embedded; IV, intravenous; K-Ras, Kirsten rat sarcoma viral oncogene homolog; mRNA, messenger ribonucleic acid; PBS, phosphate buffered saline; PECAM-1, platelet-endothelial cell adhesion molecule-1; PEG, polyethylene glycol; PPP, Pentose-phosphate pathway; RNA, ribonucleic acid; ROS, reactive oxygen species; siRNA, small-interfering RNA; TIGAR, TP53-induced glycolysis and apoptosis regulator; TP53, tumor protein p53; VEGFR2, vascular endothelial growth factor receptor 2.

Data Sharing Statement

All data are contained within the article.

Ethics Statement

All research involving vertebrate animals was performed in accordance with protocol A21-001-HARR which was approved by the Southern Methodist University-Institutional Animal Care & Use Committee. The SMU IACUC follows the ethical guidelines for vertebrate animal research as set forth by the National Institutes of Health (NIH), Office of Laboratory Animal Welfare (OLAW) – 2015 Public Health Service (PHS) Policy on Humane Care and Use of Laboratory Animals and the 2020 American Veterinary Medical Association (AVMA) Guidelines for the Euthanasia of Animals. The de-identified, primary colorectal adenocarcinoma clinical samples were collected with a waiver of consent and provided by the Pathology Core Laboratory of the University of Hawaii Cancer Center. The decision of a waiver of consent and the determination that this study (CHS #22431) is exempt were made by the University of Hawaii-Human Studies Program per Code of Federal Regulations (CFR) 45CFR 46.101(b) (Exempt Category 4) and was also approved by the SMU Human Subjects Research-Institutional Review Board under a protocol (#2016-019-HARR) that complies with Declaration of Helsinki principles.

Acknowledgments

The authors thank the Pathology Core Laboratory of the University of Hawaii Cancer Center for providing the primary colorectal carcinoma clinical samples to support these studies. We also thank Kylie James for assistance with preparing and immunostaining the tissue sections for analysis by immunoconfocal microscopy.

Funding

This study was supported by a SMU Dedman College of Humanities and Sciences Dean's Research Council grant and National Cancer Institute/National Institutes of Health grant 1R15CA267892-01A1 to RH.

Disclosure

Robert Harrod designed the siRNA-biopolymer TI6752. All other authors report no conflicts of interest in this work.

References

1. Jaworska M, Szczudlo J, Pietrzyk A, et al. The Warburg effect: a score for many instruments in the concert of cancer and cancer niche cells. *Pharmacol Rep*. 2023;75:876–890. doi:10.1007/s43440-023-00504-1
2. Liu X, Zhao Y, Wu X, Liu Z, Liu X. A novel strategy to fuel cancer immunotherapy: targeting glucose metabolism to remodel the tumor microenvironment. *Front Oncol*. 2022;12:931104. doi:10.3389/fonc.2022.931104
3. Wang Y, Patti GJ. The Warburg effect: a signature of mitochondrial overload. *Trends Cell Biol*. 2023;33:1014–1020. doi:10.1016/j.tcb.2023.03/013
4. Zhu J, Thompson CB. Metabolic regulation of cell growth and proliferation. *Nat Rev Mol Cell Biol*. 2019;20:436–450. doi:10.1038/s41580-019-0123-5
5. Zeng W, Long X, Liu PS, Xie X. The interplay of oncogenic signaling, oxidative stress and ferroptosis in cancer. *Int J Cancer*. 2023;153:918–931. doi:10.1002/ijc.34486
6. Vata O, Wade M, Kern S, et al. c-Myc can induce DNA damage, increase reactive oxygen species, and mitigate p53 function: a mechanism for oncogene-induced genetic instability. *Mol Cell*. 2002;9:1031–1044. doi:10.1016/s1097-2765(02)00520-8
7. Sagun KC, Carcamo JM, Golde DW. Antioxidants prevent oxidative DNA damage and cellular transformation elicited by the over-expression of c-MYC. *Mutat Res*. 2006;593:64–79. doi:10.1016/j.mrfmmm.2005.06.015
8. Llobet SG, Bhattacharya A, Everts M, et al. An mRNA expression-based signature for oncogene-induced replication-stress. *Oncogene*. 2022;41:1216–1224. doi:10.1038/s41388-021-02162-0
9. Srinivasan SV, Dominguez-Sola D, Wang LC, et al. Cdc45 is a critical effector of myc-dependent DNA replication stress. *Cell Rep*. 2013;3:1629–1639. doi:10.1016/j.celrep.2013.04.02
10. Edwards-Hicks J, Su H, Mangolini M, et al. MYC sensitizes cells to apoptosis by driving energetic demand. *Nat Commun*. 2022;13:4674. doi:10.1038/s41467-022-32368-z
11. Binet R, Ythier D, Robles AI, et al. WNT16B is a new marker of cellular senescence that regulates p53 activity and the phosphoinositide 3-kinase/AKT pathway. *Cancer Res*. 2009;69:9183–9191. doi:10.1158/0008-5472.CAN-09-1016
12. Liu HS, Chen CY, Chou YI. Selective activation of oncogenic Ha-ras-induced apoptosis in NIH/3T3 cells. *Br J Cancer*. 1998;77:1777–1786. doi:10.1038/bjc.1998.296
13. Campaner S, Doni M, Hydbring P, et al. Cdk2 suppresses cellular senescence induced by the c-myc oncogene. *Nat Cell Biol*. 2010;12:54–59. doi:10.1038/ncb2004

14. Menssen A, Epanchintsev A, Lodygin D, et al. c-MYC delays prometaphase by direct transactivation of MAD2 and BubR1: identification of mechanisms underlying c-MYC-induced DNA damage and chromosomal instability. *Cell Cycle*. 2007;6:339–352. doi:10.4161/cc.6.3.3808
15. Lin CY, Loven J, Rahl PB, et al. Transcriptional amplification in tumor cells with elevated c-MYC. *Cell*. 2012;151:56–67. doi:10.1016/j.cell.2012.08.026
16. Bensaad K, Tsuruta A, Selak MA, et al. TIGAR, a p53-inducible regulator of glycolysis and apoptosis. *Cell*. 2006;126:107–120. doi:10.1016/j.cell.2006.05.036
17. Cheung EC, Ludwig RL, Vousden KH. Mitochondrial localization of TIGAR under hypoxia stimulates HK2 and lowers ROS and cell death. *Proc Natl Acad Sci USA*. 2012;109:20491–20496. doi:10.1073/pnas.1206530109
18. Bensaad K, Cheung EC, Vousden KH. Modulation of intracellular ROS levels by TIGAR controls autophagy. *EMBO J*. 2009;28:3015–3026. doi:10.1038/emboj.2009.242
19. Cheung EC, Athneos D, Lee P, et al. TIGAR is required for efficient intestinal regeneration and tumorigenesis. *Dev Cell*. 2013;25:463–477. doi:10.1016/j.devcel.2013.05.001
20. Cheung EC, Lee P, Ceteci F, et al. Opposing effects of TIGAR- and RAC1-derived ROS on Wnt-driven proliferation in the mouse intestine. *Genes Dev*. 2016;30:52–63. doi:10.1101/gad.271130.115
21. Romeo M, Hutchison T, Malu A, et al. The human T-cell leukemia virus type-1 $p30^{II}$ protein activates p53 and induces the TIGAR and suppresses oncogene-induced oxidative stress during viral carcinogenesis. *Virology*. 2018;518:103–115. doi:10.1016/j.virol.2018.02.010
22. Hutchison T, Malu A, Yapindi L, et al. The TP53-induced glycolysis and apoptosis regulator mediates cooperation between HTLV-1 $p30^{II}$ and the retroviral oncoproteins Tax and HBZ and is highly expressed in an in vivo xenograft model of HTLV-1-induced lymphoma. *Virology*. 2018;520:39–58. doi:10.1016/j.virol.2018.05.007
23. Yapindi L, Bowley T, Kurtaneck N, et al. Activation of p53-regulated pro-survival signals and hypoxia-independent mitochondrial targeting of TIGAR by human papillomavirus E6 oncoproteins. *Virology*. 2023;585:1–20. doi:10.1016/j.virol.2023.05.004
24. Harrod R, Bowley H, Malu A, et al. The HTLV-1 latency-maintenance factor $p30^{II}$ induces the phosphorylation and hypoxia-independent mitochondrial targeting of TIGAR analogous to tyrosine kinase receptor-signaling and suppresses oncogene-induced oxidative toxicity. *J Antivir Antiretrovir*. 2024;16(3):313. doi:10.35248/1048-5964.16.313
25. Wang H, Wang Q, Cai G, et al. Nuclear TIGAR mediates an epigenetic and metabolic autoregulatory loop via NRF2 in cancer therapeutic resistance. *Acta Pharm Sin B*. 2022;12:1871–1884. doi:10.1016/j.apsb.2021.10.015
26. Yu HP, Xie JM, Li B, et al. TIGAR regulates DNA damage and repair through pentosephosphate pathway and Cdk5-ATM pathway. *Sci Rep*. 2015;5:9853. doi:10.1038/screp09853
27. Keller F, Bruch R, Schneider R, et al. A scaffold-free 3-D co-culture mimics the major features of the reverse Warburg effect in vitro. *Cells*. 2020;9:1900. doi:10.3390/cells9081900
28. Ahmad R, Alam M, Hasegawa M, et al. Targeting MUC1-C inhibits the AKT-S6K1-eIF4A pathway regulating TIGAR translation in colorectal cancer. *Mol Cancer*. 2017;16:33. doi:10.1186/s12943-017-0608-9
29. Cancer Genome Atlas Research Network. Integrated genomic and molecular characterization of cervical cancer. *Nature*. 2017;543:378–384. doi:10.1038/nature21386
30. Wang X, Li R, Chen R, et al. Prognostic values of TIGAR expression and 18F-FDG PET/CT in clear cell renal cell carcinoma. *J Cancer*. 2020;11:1–8. doi:10.7150/jca.33442
31. Liu Z, Wu Y, Zhang Y, et al. TIGAR promotes tumorigenesis and protects tumor cells from oxidative and metabolic stresses in gastric cancer. *Front Oncol*. 2019;9:1258. doi:10.3389/fonc.2019.01258
32. Wong EYL, Wong SCC, Chan CML, et al. TP53-induced glycolysis and apoptosis regulator promotes proliferation and invasiveness of nasopharyngeal carcinoma cells. *Oncol Lett*. 2015;9:569–574. doi:10.3892/ol.2014.2797
33. Huang S, Yang Z, Ma Y, et al. miR-101 enhances cisplatin-induced DNA damage through decreasing nicotinamide adenine dinucleotide phosphate levels by directly repressing TP53-induced glycolysis and apoptosis regulator expression in prostate cancer cells. *DNA Cell Biol*. 2017;36:303–310. doi:10.1089/dna.2016.3612
34. Chu J, Niu X, Chang J, et al. Metabolic remodeling by TIGAR overexpression is a therapeutic target in esophageal squamous-cell carcinoma. *Theranostics*. 2020;10:3488–3502. doi:10.7150/thno.41427
35. Pena-Rico MA, Calvo-Vidal MN, Villalonga-Planells R, et al. TP53 induced glycolysis and apoptosis regulator (TIGAR) knockdown results in radiosensitization of glioma cells. *Radiother Oncol*. 2011;101:132–139. doi:10.1016/j.radonc.2011.07.002
36. Li L, Liu W, Sun Q, et al. Decitabine downregulates TIGAR to induce apoptosis and autophagy in myeloid leukemia cells. *Oxid Med Cell Longev*. 2021;2021:8877460. doi:10.1155/2021/8877460
37. Yin L, Kosugi M, Kufe D. Inhibition of MUC1-C oncoprotein induces multiple myeloma cell death by down-regulating TIGAR expression and depleting NADPH. *Blood*. 2012;119:810–816. doi:10.1182/blood-2011-07-369686
38. Shen M, Zhao X, Zhao L, et al. Met is involved in TIGAR-regulated metastasis of non-small-cell lung cancer. *Mol Cancer*. 2018;17:88. doi:10.1186/s12943-018-0839-4
39. Yapindi L, Hernandez BY, Harrod R. siRNA-inhibition of TIGAR hypersensitizes human papillomavirus-transformed cells to apoptosis induced by chemotherapy drugs that cause oxidative stress. *J Antivir Antiretrovir*. 2021;13:223. doi:10.35248/1948-5964.21.13.223
40. Ye L, Zhao X, Lu J, et al. Knockdown of TIGAR by RNA interference induces apoptosis and autophagy in HepG2 hepatocellular carcinoma cells. *Biochem Biophys Res Commun*. 2013;437:300–306. doi:10.1016/j.bbrc.2013.06.072
41. Agca CA, Kirici M, Nedvetsky VS, et al. The effect of TIGAR knockdown on apoptotic and epithelial-mesenchymal markers expression in doxorubicin-resistant non-small cell lung cancer A549 cell lines. *Chem Biodivers*. 2020;17:e2000441. doi:10.1002/cbdv.202000441
42. Zhang Y, Chen F, Tai G, et al. TIGAR knockdown radiosensitizes TrxR1-overexpressing glioma in vitro and in vivo via inhibiting Trx1 nuclear transport. *Sci Rep*. 2017;7:42928. doi:10.1038/srep42928
43. Maurer GD, Heller S, Wanka C, Rieger J, Steinbach JP. Knockdown of the TP53-induced glycolysis and apoptosis regulator (TIGAR) sensitizes glioma cells to hypoxia, irradiation and temozolomide. *Int J Mol Sci*. 2019;20:1061. doi:10.3390/ijms20051061
44. Qian S, Li J, Hong M, et al. TIGAR cooperated with glycolysis to inhibit the apoptosis of leukemia cells and associated with poor prognosis in patients with cytogenetically normal acute myeloid leukemia. *J Hematol Oncol*. 2016;9:128. doi:10.1186/s13045-016-0360-4

45. Wang D, Li Y, Yang H, et al. Disruption of TIGAR-TAK1 alleviates immunopathology in a murine model of sepsis. *Nat Commun*. 2024;15:4340. doi:10.1038/s41467-024-48708-0
46. Fu J, Yu S, Zhao X, et al. Inhibition of TIGAR increases exogenous p53 and cisplatin combination sensitivity in lung cancer cells by regulating glycolytic flux. *Int J Mol Sci*. 2022;23:16034. doi:10.3390/ijms232416034
47. Pettersen EF, Goddard TD, Huang CC, et al. UCSF Chimera –a visualization system for exploratory research and analysis. *J Comput Chem*. 2004;25:1605–1612. doi:10.1002/jcc.20084
48. Boutard N, Bialas A, Sabiniarz A, et al. Synthesis of amide and sulfonamide substituted N-aryl-6-aminoquinoxalines as PFKB3 inhibitors with improved physiochemical properties. *Bioorg Med Chem Lett*. 2019;29:646–653. doi:10.1016/j.bmcl.2018.12.034
49. Feng J, Luo L, Liu Y, et al. TP53-induced glycolysis and apoptosis regulator is indispensable for mitochondria quality control and degradation following damage. *Oncol Lett*. 2018;15:155–160. doi:10.3892/ol.2017.7303
50. Li M, Sun M, Cao L, et al. A TIGAR-regulated metabolic pathway is critical for protection of brain ischemia. *J Neurosci*. 2014;34:7458–7471. doi:10.1523/JNEUROSCI.4655-13.2014
51. Liu M, Zhou X, Li Y, et al. TIGAR alleviates oxidative stress in brain with extended ischemia via a pentose phosphate pathway-independent manner. *Redox Biol*. 2022;53:102323. doi:10.1016/j.redox.2022.102323
52. Fang P, De Souza C, Minn K, Chien J. Genome-scale CRISPR knockout screen identifies TIGAR as a modifier of PARP inhibitor sensitivity. *Commun Biol*. 2019;2:335. doi:10.1038/s42003-019-0580-6
53. He X, Zeng H, Cantrell AC, Chen JX. Regulatory role of TIGAR on endothelial metabolism and angiogenesis. *J Cell Physiol*. 2021;236:7578–7590. doi:10.1002/jcp.30401
54. Hennigs JK, Cao A, Li CG, et al. PPARg-p53-mediated vasculoregenerative program to reverse pulmonary hypertension. *Circ Res*. 2021;128:401–418. doi:10.1161/CIRCRESAHA.119.316339
55. Rawat PS, Jaiswal A, Khurana A, et al. Doxorubicin-induced cardiotoxicity: an update on the molecular mechanism and novel therapeutic strategies for effective management. *Biomed Pharamacother*. 2021;139:111708. doi:10.1016/j.biopha.2021.111708
56. Lu C, Wei J, Gao C, et al. Molecular signaling pathways in doxorubicin-induced nephrotoxicity and potential therapeutic agents. *Int Immunopharmacol*. 2025;144:113373. doi:10.1016/j.intimp.2024.113373
57. Elmorsy EA, Saber S, Hamad RS, et al. Advances in understanding cisplatin-induced toxicity: molecular mechanisms and protective strategies. *Eur J Pharm Sci*. 2024;203:106939. doi:10.1016/j.ejps.2024.106939
58. Jang JY, Kim D, Im E, et al. Etoposide as a key therapeutic agent in lung cancer: mechanisms, efficacy, and emerging strategies. *Int J Mol Sci*. 2025;26:796. doi:10.3390/ijms26020796
59. Wang J, Cui J, Hao T, et al. Regulation of cyclophosphamide induced hepatotoxicity by REV-ERBa modifiers. *Expert Opin Drug Metab Toxicol*. 2025;11:1–11. doi:10.1080/17425255.2025.2490741
60. Bhattacharjee P, Wang D, Anderson D, et al. The immune response to RNA suppresses nucleic acid synthesis by limiting ribose 5-phosphate. *EMBO J*. 2024;43:2636–2660. doi:10.1038/s44318-024-00100-w